Numerical Solution for the Near Wake of a Body with Propeller

Joseph A. Schetz* and Stanley Favin†
Applied Physics Laboratory, Johns Hopkins University, Laurel, Md.

A numerical solution of the Navier-Stokes equations applied to the tail and near wake region of a slender, axisymmetric body with a stern-mounted propeller is presented. The propeller is modeled as an actuator zone which may be arbitrarily arranged in space with an arbitrary radial distribution of thrust. The turbulence exchange processes are described by an integrated, turbulent-kinetic-energy equation. The unsteady equations are cast in terms of the vorticity and a stream function. The vorticity equation is solved by an ADI method, and the stream function equation is solved by direct matrix reduction.

Nomenclature

a_2 = constant in turbulence model
b = mixing zone width
c_2 = constant in turbulence model
F_x = thrust per unit area
H = height of the calculation region
i = index for grid points in the axial direction
j = index for grid points in the radial direction
I_1, I_2 = integrals in TKE equation
k = turbulent kinetic energy (TKE)
n = index for time step
r = radial coordinate
$\bar{r}$ $\equiv r/b$
t = time
u = axial velocity
$\bar{u}$ $\equiv u/U_e$
$U_e(x)$ = edge velocity
U_∞ = free-stream velocity
v = radial velocity
x = axial coordinate
ξ = vorticity
ψ = stream function
ϵ = eddy viscosity
ρ = density
τ = shear
δ_r^* = displacement thickness

Subscripts

b, w = on the body

Introduction

PREDICTIONS of the performance and flowfield influence of a propeller are of interest in a number of engineering applications. Typical examples include the influence of a tail-mounted propeller on the surface pressure distribution and boundary-layer flow in the stern region of a ship or submarine, and the generation of the near-field wake for the same general arrangement.

As a result of the existence of these practical applications, approximate analyses have been developed over a number of years. References 1, 2, and 3 are representative. Works of this type generally involve one or more of the following assumptions: the flow is taken as inviscid; the propeller is assumed to be an actuator disk with spatially constant thrust; the flow is laminar; and the effects of the propeller on the flowfield are small enough to permit a linearization of the equations of motion. While some useful results can be obtained from such treatments, many important phenomena cannot be properly accounted for.

The work reported here has as its goal the development of a realistic treatment of the flow near a propeller, holding simplifying assumptions and approximations to a minimum. Since upstream influence effects are clearly of importance, a boundary-layer equation formulation is inappropriate. It was decided to employ the full Navier-Stokes equations rather than attempt to develop some ad hoc approximate system that would fall somewhere between the full equations and a boundary-layer approximation. Also, since all practical systems involve turbulent flow, a reasonable, but not overly elaborate, turbulent transport model was deemed necessary. Our reservation concerning the immediate application of one of the existing, very elaborate turbulence models in the literature stems primarily from the dearth of required experimental turbulence information for the problems of interest here.

In order to place some bounds upon the scope of the effort, some simplifications were necessary. The first of these is the assumption of an actuator disk model for the propeller, although arbitrary radial variations of thrust are allowed. The actuator disk model is a direct result of avoiding the great additional complexity of the periodic, unsteady formulation required to treat individual propeller blades. Also, the propeller can be arbitrarily located in space, so that the effects of rake, etc, can be investigated in detail. Second, at this point in the work, swirl has been assumed negligible. This assumption is removable by relatively direct means within the general actuator disk model, and we intend to do so in the future.

Once the framework of the problem as described above was determined, the next item of importance was the selection of a mathematical/numerical formulation. In this, we were guided by the efforts of Briley[4] concerning the treatment of an isolated separation bubble. The two flow problems are similar in that they both involve a fully elliptic region, a separation region in one and a propeller region in the other, imbedded within a generally parabolic flow problem. The flow over most of a stern-propeller-driven body and far in its wake can be treated by parabolic methods. The same is true for boundary-layer flow upstream and downstream of an isolated separation bubble. The main items carried over from Briley's approach were the selection of an unsteady, vorticity-stream function, mathematical fomulation, and specification of the boundary conditions, especially on the downstream boundary.

Received Oct. 22, 1976; revision received March 14, 1977.
Index categories: Hydrodynamics; Jets, Wakes and Viscid-Inviscid Flow Interactions; Marine Propulsion.

*Consultant, also Professor and Dept. Head, Aerospace and Ocean Engineering Dept., Virginia Polytechnic Institute and State University. Associate Fellow AIAA.
†Senior Programmer.

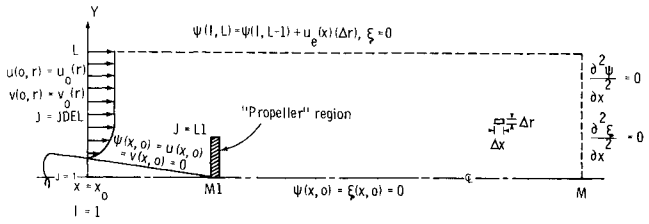

Fig. 1 Schematic of the flowfield and the computational approach.

The boundary conditions used here are shown in Fig. 1 which is a schematic of the flow problem treated. The body is taken as slender with a propeller at the stern. On the upstream boundary, the velocity profile is completely specified. This would presumably come from a boundary-layer solution of the upstream flow. This boundary must be located ahead of the region of upstream influence of the propeller. On the outer boundary, the vorticity is taken as zero, and the stream function is calculated assuming $u = U_e(x)$. The edge velocity distribution $U_e(x)$ is calculated from a basic potential-flow inviscid solution which is then perturbed repeatedly by an inviscid-viscous iteration procedure as the solution progresses in time. On the body, the velocity and the stream function are taken as zero, and the wall vorticity must be determined iteratively. The details of these last two matters will be presented in later sections. The flow on the axis behind the body is specified by zero vorticity and stream function.

The conditions to be employed on the downstream boundary of problems of this general type have been the subject of some debate (see Ref. 5 for a discussion). Briley[4] apparently was the first to propose the use of zero axial second derivatives for both the stream function and the vorticity. Such a choice is perfectly suitable from a mathematical viewpoint and has the added physical appeal that it specifies the end of the elliptic region and the beginning of a parabolic region. This, of course, is precisely when one would wish to terminate an elliptic calculation in any event. The actual location of a suitable downstream boundary must be determined somewhat empirically.

A major difference between the general numerical approach used here and that used by Briley is our adoption of a direct solver procedure for the stream function equation.[6,7] This results in a substantial reduction in computational time and the elimination of the vague arbitrariness associated with terminating iterative solutions. The vorticity equation is still treated by the alternating-difference-implicit (ADI) procedure.[8]

Analysis

Equations

Assuming that the flow is axisymmetric and unsteady, the Navier-Stokes equations and the definition of vorticity may be written as

$$\frac{\partial \xi}{\partial t} + u\frac{\partial \xi}{\partial x} + v\frac{\partial \xi}{\partial y} - \frac{v\xi}{r} = \epsilon\left(\frac{\partial^2 \xi}{\partial r^2} + \frac{1}{r}\frac{\partial \xi}{\partial r} + \frac{\partial^2 \xi}{\partial x^2} - \frac{\xi}{r^2}\right) + \frac{1}{\rho}\frac{\partial F_x}{\partial r} \tag{1}$$

$$\frac{\partial^2 \psi}{\partial r^2} + \frac{\partial^2 \psi}{\partial x^2} - \frac{1}{r}\frac{\partial \psi}{\partial r} = r\xi \tag{2a}$$

The velocity components can be determined from

$$ur = \frac{\partial \psi}{\partial r}\,; \quad vr = \frac{-\partial \psi}{\partial x} \tag{2b}$$

Here, we have written the equations with a constant turbulent eddy viscosity ϵ only for simplicity of the presentation. Actually, a variable eddy viscosity was employed in most calculations, as will be described later. The propeller appears through the axial force term F_x which may be an arbitrary, but differentiable function of r.

Boundary and Initial Conditions

As discussed in the Introduction and shown in Fig. 1, the boundary conditions used may be written as

$$\begin{aligned} u(0,r) &= u_o(r) \\ v(0,r) &= v_o(r) \\ \xi(x,H) &= 0 \\ \psi(x,H) &= \psi(x,H-\Delta r) + U_e(x)\cdot(\Delta r) \end{aligned}$$

$$\frac{\partial^2 \xi}{\partial x^2}(x_f,r) = \frac{\partial^2 \psi}{\partial x^2}(x_f,r) = 0$$

$$\begin{aligned} \psi(x,r_b) &= 0 && \text{all } x \\ \xi(x,r_b) &= 0 && x > x_1 \\ u(x,r_b) &= v(x,r_b) = 0 && 0 \le x \le x_1 \end{aligned}$$

The boundary conditions on the body cannot be directly restated in terms of the vorticity at the wall, so that an iterative procedure is required. Indeed, it will develop that this is the only iterative loop in the entire solution for this problem. To proceed, we first write

$$\psi(x,r_b+\Delta r) = \psi_w + \frac{\partial \psi}{\partial r}(\Delta r) + \frac{\partial^2 \psi}{\partial r^2}\frac{(\Delta r)^2}{2} + \frac{\partial^3 \psi}{\partial r^3}\frac{(\Delta r)^3}{6} + \ldots \tag{3a}$$

and

$$\psi(x+\Delta x,r_b) = \psi_w + \frac{\partial \psi}{\partial x}(\Delta x) + \frac{\partial^2 \psi}{\partial x^2}\frac{(\Delta x)^2}{2} + \frac{\partial^2 \psi}{\partial x^3}\frac{(\Delta x)^3}{6} + \ldots \tag{3b}$$

where on the body, $r = r_b$. Also

$$u = \frac{1}{r_b}\frac{\partial \psi}{\partial r}\bigg|_{r=r_b} = 0$$

$$v = -\frac{1}{r_b}\frac{\partial \psi}{\partial x}\bigg|_{r=r_b} = 0$$

and

$$\psi(x,r_b) = \psi_w = 0$$

Therefore,

$$\xi_w(x) \equiv \left(\frac{\partial u}{\partial r} - \frac{\partial v}{\partial x}\right)_{r=r_b} = \frac{2}{r_b}\left(\frac{\psi(x+\Delta x,r_b)}{(\Delta x)^2} + \frac{\psi(x,r_b+\Delta r)}{(\Delta r)^2}\right) \tag{4a}$$

At the tail of the body and also for a body of limiting small slenderness, $r_b \to 0$. In that case, the analysis is somewhat modified with the result

$$\xi_w(x) = \frac{3\psi(x,\Delta r)}{(\Delta r)^3} \tag{4b}$$

This general development is similar to that suggested for planar problems in Ref. 5.

Since an unsteady formulation is employed here to develop the desired steady-state solution, initial conditions must be

specified. To start a completely new problem with a very slender body, the vorticity and stream function distributions implied by the fixed (with time) upstream velocity profile are imposed over the entire region as an initial guess. For more general bodies, the procedure described in the next section is used. If the effects of even rather large changes on an existing calculation for a given body shape are being studied, the solution for the baseline problem is used as the starting point.

Outer Edge Boundary Conditions

The formulation adopted here requires the specification of the velocity distribution along the outer boundary. In principle, one could take the outer boundary at a large enough radius such that the uniform, freestream conditions apply. This is preferable from a mathematical viewpoint, but very costly in terms of computer storage and execution time. Thus, it is desired to have an outer boundary at a large enough radius only to be well clear of the viscous region. This will obviously still be deep in the mainly inviscid flow around the body/boundary-layer/propeller/wake system.

We have adopted the following general procedure to treat the situation. First, an exact solution to a related inviscid flow problem is taken as a base solution. This base solution is then perturbed by an inviscid-viscous interaction procedure to determine the correct velocity distribution along the outer boundary. An additional benefit arises in that the base, inviscid solution can be crudely doctored with a boundary-layer profile near the body that produces a rather good initial guess with which to begin the whole unsteady calculation.

The base, inviscid solution used here is the simple-source/line-sink/uniform-stream combination that is known to produce a streamlined body with a tapered tail.[9] The solution for the stream function can be written

$$\psi(R,\theta) = -m\cos\theta + (m'\ell)\left((R/\ell) - \sqrt{(R/\ell)^2 + 1 - 2(R/\ell)\cos\theta}\right) + \frac{1}{2}(R/\ell)^2\sin^2\theta \qquad (5)$$

where m is the source strength, m' is the sink strength per unit length and where ℓ is the length of the sink.

For a closed body, $m = m'\ell$. Eq. (5) can be written in completely nondimensional terms and this introduces the single parameter $M \equiv m/U\ell^2$. Body shapes are characterized only by the value of this parameter. We have worked with $M = 7.5 \times 10^{-4}$ and that corresponds to the body shape shown in Fig. 2. Of course, for our purposes here, only the tail region is of direct interest. The expression in Eq. (5) can be used with standard procedures to give a velocity distribution throughout the field, including the outer boundary. We call the axial velocity along this line $U_e(x)$.

The viscous zone near the body as well as the flow induced by the propeller and the wake zone will clearly perturb the real velocity distribution along the outer boundary away from the inviscid estimate described above. A simple, inviscid-viscous interaction approach based upon the profile correction treatment of Allen[10] was used. This is similar to the approach of Briley and McDonald[11] for a separation bubble, although they had no body shape or propeller to contend with. A distribution of small sources (or sinks) is placed along the body axis midway between the axial grid points. The strength of each is determined to match the newly calculated distribution of the value of the stream function along the outer boundary in comparison with that projected by the simple-source/line-sink combination approximate solution. This distribution of sources (and/or sinks) is then used to calculate a perturbation to the velocity distribution boundary condition along the outer boundary. This whole operation is performed every several (usually five) time steps.

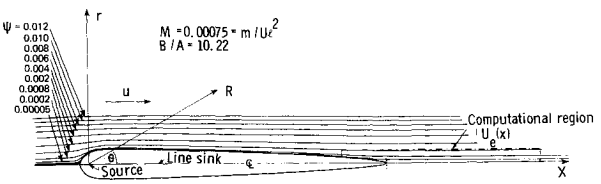

Fig. 2 The slender-body and its flowfield used as the inviscid baseline solution.

Turbulence Model

As discussed in the Introduction, a simple turbulence model was desired since there is little detailed experimental turbulence data available for this type of problem. With this viewpoint, the general approach of McDonald and Camarata[12] seemed particularly appropriate for application here. Basically, one attempts to calculate the variation of some mean flow type of exchange coefficient (an eddy viscosity or a mixing length) using an integrated form of the turbulent kinetic energy equation. Here, it has not been deemed worthwhile to try to accurately resolve the region near the body wall, so an eddy viscosity model that varied with x alone was adopted.

For an axisymmetric geometry, the integrated turbulent kinetic energy equation may be written as[13]

$$\int_0^{b(x)} \frac{\partial}{\partial x}(\rho u) r dr = \int_0^{b(x)} \tau \left(\frac{\partial u}{\partial r}\right) r dr - \frac{a_2}{b}\int_0^{b(x)} \rho k^{3/2} r dr \qquad (6)$$

Now introducing an eddy viscosity and following Prandtl's model[14]

$$\tau = \rho\epsilon \frac{\partial u}{\partial r} = \rho\sqrt{k}\ell \frac{\partial u}{\partial r} \qquad (7)$$

With $\ell = c_2 b$ and $\bar{u} = u/U_e$, $\bar{r} = r/b$, Eq. (6) becomes

$$\frac{d\epsilon(x)}{dx} = \frac{c_2^2 U_e}{2}\left(\frac{I_2}{I_1}\right) - \frac{a_2\epsilon^2}{4U_e c_2 b^2 I_1} - \frac{\epsilon}{2I_1}\frac{dI_1}{dx} + \frac{\epsilon}{2b}\frac{db}{dx} - \frac{\epsilon}{2U_e}\frac{dU_e}{dx} \qquad (8)$$

where

$$I_1(x) \equiv \int_0^1 \bar{u}\bar{r}d\bar{r} \qquad I_2(x) \equiv \int_0^1 \left(\frac{\partial \bar{u}}{\partial \bar{r}}\right)^2 \bar{r}d\bar{r} \qquad (9)$$

We have used $a_2 = 1.40$ and $c_2 = 0.035$.

Eq. (8) is employed to recalculate an eddy viscosity $\epsilon(x)$ distribution after every five time steps. A comparison of the prediction obtained using this turbulence model in a boundary-layer calculation procedure with data for a low-speed wake is shown in Fig. 3. Some studies of the effects of variations in necessary parameters are also shown.

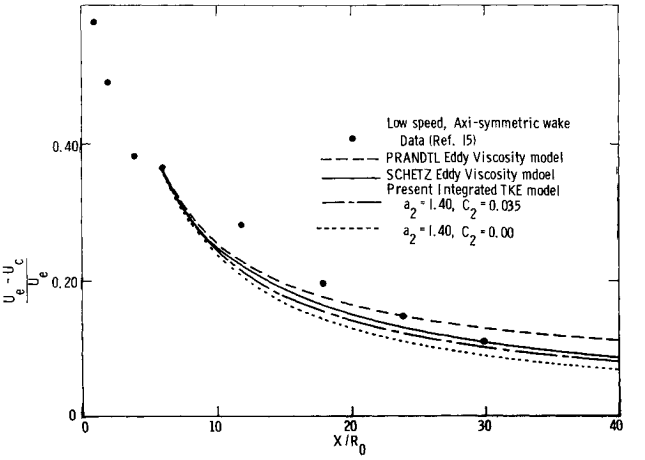

Fig. 3 Comparison of wake data and predictions using various turbulence models.

Numerical Procedures

The vorticity equation, Eq. (1), is solved for each time step Δt in two half time steps $\Delta t/2$ using the ADI method of Peaceman and Rachford.[8] The details for numerical analysis of the current axisymmetric problem are generally similar to those shown in Briley[4] for his planar problem. The resulting systems of algebraic equations were solved using a Library Subroutine, LEQT1B, obtained through IMSL.

The solution to the vorticity equation is then used pointwise for the nonhomogeneous right hand side of the stream function equation. Eq. (2). To solve this equation, the direct reduction method of Buneman[6] as implemented by Swartztrauber and Sweet[7] was employed. This is an extremely convenient and efficient procedure which does not involve the iterations that plague the various over-relaxation and ADI methods that are often applied to equations of this type. For perspective, the NCAR code was used here to solve Eq. (2) on a 60×30 grid in less than 0.01 sec on an IBM 360/91. As mentioned before, it is necessary to iterate on the boundary condition for the vorticity along the solid surface.

The entire solution procedure can best be illustrated by a step-by-step listing showing how the solution is advanced from $t=n(\Delta t)$ to $t=(n+1)(\Delta t)$:

1) Obtain boundary conditions for ξ^{n+1} and ψ^{n+1}. These are known and usually fixed with time, except for ξ_w^{n+1} which must be iterated for at each time step. The coefficients $u_{i,j}^{n+1/2}$ and $v_{i,j}^{n+1/2}$ in the difference form of Eq. (1) are obtained by extrapolation from the previous time step.

2) Solve Eq. (1) using the ADI procedure to obtain ξ^{n+1}.

3) Solve for ψ^{n+1} using the direct solver procedure from Eq. (2) with ξ^{n+1} for the right hand side.

4) Calculate new values of ξ_w^{n+1} using ψ^{n+1} and Eqs. (4a and 4b).

5) Repeat steps 2, 3, and 4 until ξ_w^{n+1} values converge.

6) Compute u^{n+1} and v^{n+1} from ψ^{n+1} using Eq. (2a).

7) Increase or decrease Δt depending upon the number of iterations required to determine ξ_w. If fewer than two iterations are required $\Delta t^{n+1}=r(\Delta t)$.

8) After every five time steps, recalculate $\epsilon(x)$ using Eq. (8) and the current velocity profiles. The value of $\epsilon(0)$ at the upstream boundary must be given as a boundary condition. We also recalculate $U_e(x)$ at this time for cases with an upstream body of finite thickness.

Results

Cases with an upstream body of vanishing thickness are simpler in that the calculation of the inviscid flowfield along the outer boundary is circumvented. We will show some results for such a case first and then move on to give some results for body shapes of more practical interest.

Very Slender Bodies

A series of systematic computations have been run for the limiting situation in Fig. 1 when the body thickness is taken as zero. The grid was 30×60 (i.e., $L=30$ and $M=60$) with $(\Delta x)>(\Delta r)$. The upstream velocity profile was chosen as $u_o(r)=(r/\delta)^{1/4}$, $v_o(r)=0$ with $\delta=(\Delta r)$(JDEL-1) and JDEL $=10$.

The propeller was located over one (or two) columns of grid points, $I=M1$ (and $M1+1$) with $J\le L1$, where $M1=15$ and $L1=12$. The axial force was distributed with radius as

$$\frac{F_x}{\rho}=F_{x_0} \qquad 0\le r\le (L1-5)\Delta r \tag{10a}$$

$$\frac{F_x}{\rho}=\frac{F_{x_0}}{2}\left\{1+\cos\left[\pi\left(\frac{r-(L1-5)(\Delta r)}{4(\Delta r)}\right)\right]\right\}$$

$$(L1-5)\Delta r\le r\le (L1-1)\Delta r \tag{10b}$$

so that the important blade tip region can be treated reasonably with a finite difference approach. This is all shown in Fig. 4. The value of F_{x_0} was chosen based upon the momentum defect of the initial velocity profile, $u_0(r)$.

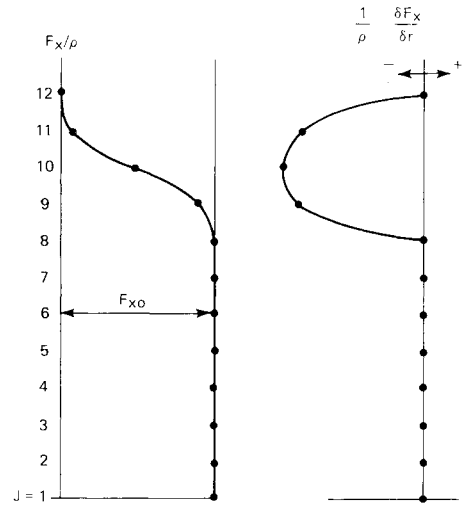

Fig. 4 Radial thrust variation used in propeller simulations.

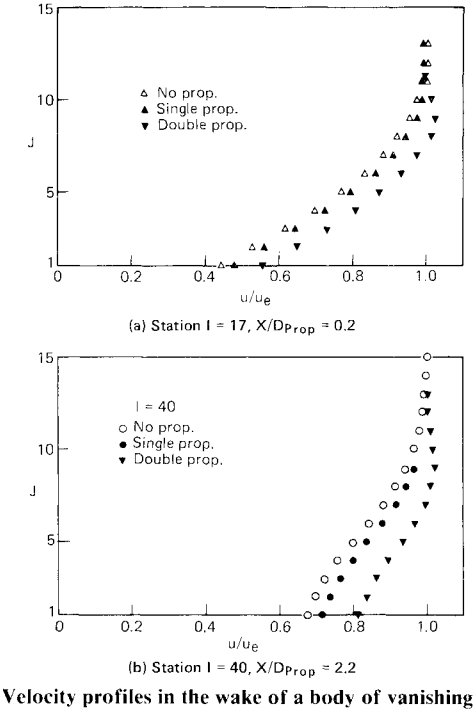

Fig. 5 Velocity profiles in the wake of a body of vanishing thickness with a propeller at the tail.

A free stream velocity, $U_\infty=10$ fps was used with a density, $\rho=60$ #/ft^3. The grid sizes were $\Delta x=0.136$ ft and $\Delta r=0.062$ ft.

The value of the eddy viscosity at the upstream boundary $\epsilon(0)$ was determined from the net displacement thickness of the profile as

$$\epsilon=0.018U_e(0)\delta_r^* \tag{11a}$$

where

$$(\delta_r^*)^2=\int_0^\delta\left(1-\frac{u}{U_e}\right)rdr \tag{11b}$$

This is similar to the approach previously used[16] with some success to give eddy viscosity values for axisymmetric wakes and jets. Of course, any other procedure could be employed to obtain a value for $\epsilon(0)$.

A series of computations were performed using a constant value of the eddy viscosity for simplicity, i.e., $\epsilon(x)=\epsilon(0)$, and

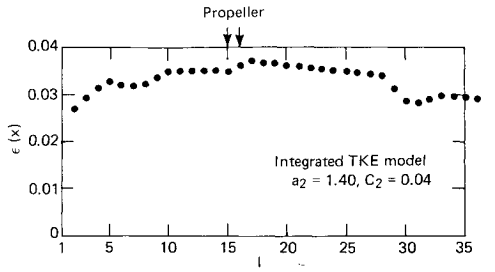

Fig. 6 Axial distribution of eddy viscosity for the body of vanishing thickness with a propeller at the tail.

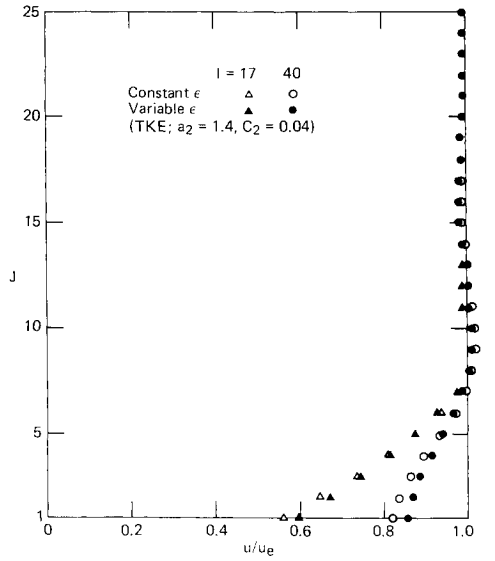

Fig. 7 Comparison of predicted velocity profiles for constant and variable eddy viscosity for the body of vanishing thickness with a propeller at the tail.

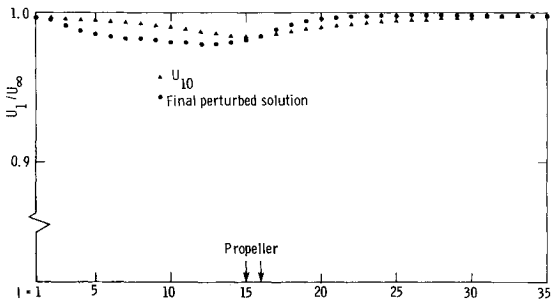

Fig. 8 The final perturbed interacted solution and the inviscid baseline solution for the velocity along the outer edge of the computational region for the 10 × 1 body with a propeller at the tail.

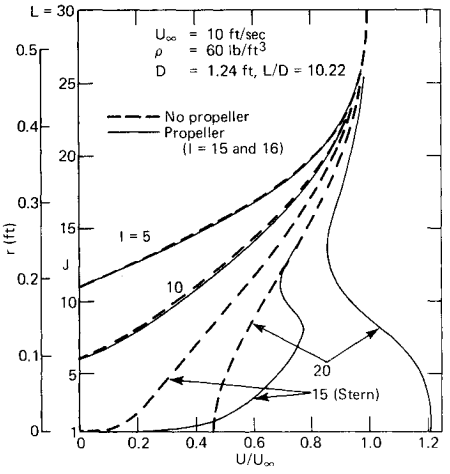

Fig. 9 Velocity profiles near the tail and in the wake of the 10 × 1 body with and without a propeller at the tail.

these will be presented first. Results in terms of axial velocity profiles at two stations are given in Figs. 5a and 5b. One station, $I=17$, is immediately behind the propeller and the second, $I=40$, is approximately two propeller diameters downstream. The open triangles indicate how the velocity profile develops for no propeller. The solid triangles show the effects of thrust in a single transverse plane (at $I=M1=15$). Here, $F_{x0}=43.3$. The inverted, solid triangles show the profiles with thrust over two transverse planes ($I=15$ and 16), with the same value of F_{x0} on each. In this case, the velocity profile overshoots the freestream velocity, and a near self-propelled condition is reached.

Next, the calculation with the two-plane propeller was rerun but with the TKE equation to calculate $\epsilon(x)$. The resulting variation of $\epsilon(x)$ is given in Fig. 6, and the velocity profiles obtained are compared with those for a constant ϵ in Fig. 7.

10 × 1 Upstream Body

Following the successful treatment of the limiting case of an upstream body of vanishing thickness as described in the preceding section, the more realistic body shown in Fig. 2 was considered in detail. The actual computational region used is also shown in Fig. 2. A basic grid of $J=1$ to 30 by $I=1$ to 60 was employed with the triangular corner $J=1$ to 15 by $I=15$ deleted to form the sharp tail of the body. The grid spacing was $\Delta x=0.136$ ft and $\Delta r=0.019$ ft. The freestream velocity, U_∞ was set at 10 fps, with the density at 60 #/ft^3.

A propeller with the same type of radial distributions as shown in Fig. 4 was employed with $F_{x0}=259$. The actuator zone was spread over $I=15(=M_1)$ and 16, and it extended radially from the axis out to $J=L1=12$.

The computation was begun with the base inviscid solution described in a previous section. The streamline pattern for this solution is also shown in Fig. 2 for reference. The flow at the upstream boundary of the computational region was modified to include a viscous layer of the form

$$\frac{u_0(r)}{u(r=\delta)}=\left(\frac{r-r_b}{\delta}\right)^{1/4} \tag{12}$$

The outer edge of the boundary layer, $r=r_b+\delta$, was taken at J = JDEL = 25 (note that the body is at $J=15$ at this station). The velocity profile at the upstream station, the boundary-layer profile in Eq. (12) and the base inviscid flow from $J=25$ to 30, is kept fixed (with time) as a constant boundary condition.

The velocity along the outer boundary, which enters into the boundary condition on the stream function, is determined via the inviscid-viscous interaction procedure described before that produces a perturbation on the base inviscid flow at the same location. The result of this whole operation is shown in Fig. 8 where we compare the final, perturbed velocity distribution with the initial, base inviscid solution. As hoped, the perturbation is indeed small.

The results in terms of axial velocity profiles at several axial stations, both ahead of and behind the propeller are shown in Fig. 9. The dashed curves are the final, viscous solution for the flow over the body in the absence of a propeller. The stations $I=5$ and 10 are on the body ahead of the propeller, and $I=15$ is located right at the point of the tail. The profiles on the body ($I=5$ and 10) are more or less typical boundary-layer profiles, and behind the body ($I=20$) is a typical wake profile. The profile at the tail ($I=15$) is an interesting combination of the two types. One can see the upstream influence of the wake in the outer part of the profile.

The velocity profiles calculated in the presence of the propeller are shown as solid curves on Fig. 8. There is a negligible upstream influence of the propeller on the profile at $I=5$. The first is approximately 1.3 propeller diameters upstream of the propeller. The velocity profile behind the propeller ($I=20$) is radically changed from that without the propeller. The velocity on the axis is accelerated to a value 20% greater than the freestream, and a nearly self-propelled condition is indicated. A very complicated profile is predicted for the $I=15$ station which is now in the plane of the propeller itself.

Further Observations on the Solutions

A study of the effect of grid sizing on the resulting solutions was made for the last problem treated and described above. To this end, calculations were run with Δx and Δr reduced to half their original size. Of course, considerably greater computer storage and execution time were required for each time step. The calculation was started with the steady-state solution obtained from the coarser grid computation, and it was run for 10 time steps. Essentially no difference was found between the coarser and finer grid solutions. This serves to justify the grid sizing chosen originally and to provide guidance for future computations.

An interesting phenomena was observed when running the dual-transverse-plane propeller case starting with the single-transverse-plane propeller case, steady-state solution. Small wiggles appeared in the solution for the vorticity equation as the influence of the increased propeller thrust washed downstream. Happily, these wiggles decreased steadily in magnitude with time. However, this phenomena did seem to increase the calculation time required to reach a final steady state.

Discussion

The flow at the rear of a slender body with a stern-mounted propeller has been treated with a numerical solution of the Navier-Stokes equations. Turbulent transport was modeled with an eddy viscosity calculated using an integrated TKE equation. This procedure produced eddy viscosity variations that varied continuously, but not greatly, over the flowfield.

An unsteady formulation was used to calculate the desired steady-state results. For a completely new problem starting from a crude initial guess, approximately 50 time steps were required. This consumed about 40 seconds of step time on the APL IBM 360/91 for a 30×60 grid. For cases where a good initial guess was available, such as in going from a propeller over one transverse plane to over two planes, only about 15 time steps were required to reach steady state.

Cases with an upstream body with a pointed tail produced interesting results both with and without a stern mounted propeller. Both situations showed important upstream influence effects that can only be predicted using a fully elliptic formulation such as that used here. For the case with no propeller, the wake-like character of the velocity profiles right near the tail demonstrates that the downstream wake communicates with the flow on the body. For cases with a propeller located at the tail, the velocity profiles on the body just ahead of the tail show an accelerated flow induced by the propeller.

Acknowledgment

This work was supported by U.S. Navy Contract N00017-72-C-4401.

References

[1] Von Karman, T. and Burgers, J. M., "General Aerodynamic Theory-Perfect Fluids," *Aerodynamic Theory*, Vol. II, California Institute of Technology, 1934, pp. 104-112.

[2] Sparenberg, J. A., "On the Potential Theory of the Interaction of an Actuator Disk and a Body," *Journal of Ship Research*, Vol. 16, Dec. 1972, pp.271-277.

[3] Sparenberg, J. A., "On the Linear Theory of an Actuator Disk in a Viscous Fluid," *Journal of Ship Research*, Vol. 18, March 1974, pp.16-21.

[4] Briley, W. R., "A Numerical Study of Laminar Separation Bubbles Using the Navier-Stokes Equations," *Journal of Fluid Mechanics*, Vol. 47, 1971, pp.713-736.

[5] Roach, P. J., *Computational Fluid Dynamics*, Hermosa Publications, Albuquerque, 1972.

[6] Buzbee, B., Dorr, F., George, J. and Golub, G., "The Direct Solution of the Discrete Poisson Equation on Irregular Regions," *SIAM Journal of Numerical Analysis*, Vol. 8, 1971, pp.722-736.

[7] Swartztrauber, P. and Sweet, R., "Efficient FORTRAN Subprograms for the Solution of Elliptic Partial Differential Equations," NCAR TN/IA-109, 1975.

[8] Peaceman, D. W., and Rachford, H. H., "The Numerical Solution of Parabolic and Elliptic Differential Equations," *SIAM Journal*, Vol. 3, 1955, pp.28-41.

[9] Vallentine, H. R., *Applied Hydrodynamics*, Plenum Press, New York, 1967, p. 250.

[10] Allen, H. J., "General Theory of Airfoil Sections Having Arbitrary Shape or Pressure Distribution," NACA Rept. 833, 1945.

[11] Briley, R. and McDonald, H., "Numerical Prediction of Incompressible Separation Bubbles," *Journal of Fluid Mechanics*, Vol. 69, 1975, pp.631-656.

[12] McDonald, H. and Camarata, F. J., "An Extended Mixing Length Approach for Computing Turbulent Boundary Layer Development," AFOSR-IFP Stanford Conference on Turbulent Boundary Layer Prediction, Stanford, Calif., 1968.

[13] Peters, C. and Phares, W. J., "An Integral Turbulent Kinetic Energy Analysis of Free Shear Flows," NASA SP-321, 1971.

[14] Prandtl, L., "Über ein neues Formelsystem der ausgebildeten Turbulenz," *Nachrichten der Akademie der Wissenschafter Gottingen*, Vol. 6, 1945.

[15] Chevray, R., "The Turbulent Wake of a Body of Revolution," *Journal of Basic Engineering*, Vol. 90, June 1968, pp.275-284.

[16] Schetz, J. A., "Turbulent Mixing of a Jet in a Co-flowing Stream," *AIAA Journal*, Vol. 6, Oct. 1968, pp. 2008-2010.